A. B. Palazzolo

S. Jagannathan

Texas A&M University,
College Station, TX

A. F. Kascak
U.S. Army at NASA Lewis

G. T. Montague
Sverdrup at NASA Lewis

L. J. Kiraly
NASA Lewis

Hybrid Active Vibration Control of Rotorbearing Systems Using Piezoelectric Actuators

The vibrations of a flexible rotor are controlled using piezoelectric actuators. The controller includes active analog components and a hybrid interface with a digital computer. The computer utilizes a grid search algorithm to select feedback gains that minimize a vibration norm at a specific operating speed. These gains are then downloaded as active stiffnesses and dampings with a linear fit throughout the operating speed range to obtain a very effective vibration control.

Introduction

Active vibration control has become an area of intense research in rotorbearing systems, machine tools, large space structures, and in robotics. Significant efforts are being made to apply active vibration control (AVC) devices to rotating machinery in the petrochemical, aerospace, and power utility industries. The advantages of active control over passive, i.e., absorber and dampers, is the versatility of active control in adjusting to a myriad of load conditions and machinery configurations. This is clearly illustrated when one considers the very narrow bandwidth that a tuned spring mass absorber is effective in. Other possible advantages that have been cited for AVC include compact size, light weight, no lubrication systems needed in the control components, and operation in high or low temperature environments.

In this paper an algorithm has been developed for performing a computer directed grid search to identify the best feedback gains for a piezoelectric-actuator based active vibration control system. These gains are stored in an array for a shaft speed interval covering the operating range. The feedback gains are automatically downloaded versus speed for all successive runs of the test rig.

Literature Review

Electromagnetic shakers and magnetic bearings have been used for actuators in the majority of the active vibration control research mentioned in the literature. Magnetic bearings force the rotor without contact while electromagnetic actuators apply forces to the rotor indirectly through the bearings. Salm and Schweitzer (1984) examined the stability and observability of rotorbearing systems with active vibration control, and presented an analysis which related force and stiffness to electrical and geometrical properties of electromagnetic bearings.

Nikolajsen (1979) examined the application of magnetic dampers to a 3.2 meter simulated marine propulsion system. Gondhalekar and Holmes (1984) suggested that electromagnetic bearings be employed to shift critical speeds by altering the suspension stiffness. Weise (1985) discussed proportional, integral, derivative (PID) control of rotor vibrations and illustrated how magnetic bearings could be used to balance a rotor by forcing it to spin about its inertial axis. Humphris et al. (1986) compared predicted and measured stiffness and damping coefficients for a magnetic journal bearing.

Several papers describe active vibration control utilizing other types of actuators such as pneumatic, hydraulic, electrohydraulic, and eddy current force generators. Ulbrich and Althaus (1989) discussed the advantages and disadvantages of different types of actuators, and examined controlled hydraulic chambers as force actuators. This compact system could develop very large forces and thereby influence even large turbines weighing several tons; however, the difficulty of hydraulic control lies in high frequency response, which was essentially limited by the servo valve implemented and fluid losses. Feng (1986) developed an active vibration control scheme with actuator forces resulting from varying bearing oil pressure. Heinzmann (1980) employed loud speaker coils linked to the shaft via ball bearings to control vibrations.

Crawley and de Luis (1983, 1985) used piezoceramics, bonded on the surface of cantilever beams, as actuators either to excite vibrations or to suppress the vibrations by introducing damping to the system. Furthermore, they developed a theoretical background for predicting the amplitude of the vibration induced by piezoceramics. Stjernstrom (1987) bonded piezoceramics on cantilever beams as actuators and sensors to induce the 1st and 2nd vibration modes.

Contributed by the Technical Committee on Vibration and Sound for publication in the JOURNAL OF VIBRATION AND ACOUSTICS. Manuscript received Oct. 1991. Associate Technical Editor: H. Nelson.

Matsubara et al. (1989) employed piezoelectric dampers to suppress chatter vibration during a boring process. These piezoelectric dampers were driven so as to generate damping forces corresponding to the vibration velocity of the boring bar. Tzou (1987) demonstrated the control of bending vibration in nonrotating beams by using layered piezoelectric materials.

Palazzolo et al. (1989a, 1989b) and Lin (1990, 1991) derived simulation models and demonstrated test results of active vibration control of rotorbearing system utilizing piezoelectric pushers as actuators. The correlations for unbalance response and transient response between the predicted and test results was very good. The piezoelectric actuators are represented by equivalent, linear electric circuits with components selected so as to match the frequency response function of the circuit to that of the actuator. The differential equations for the circuits were assembled into structural matrices to form an electromechanical model of the system. This model was then employed to predict instability onset feedback gains, total system stability, and total system forced response. The results showed very good agreement between test and theory for unbalanced response and for the instability onset gain with derivative feedback. The current paper extends this work by presenting a methodology to automatically select and down-load feedback gains (active stiffnesses and dampings) based on minimizing a user defined norm of measured rotor vibration. The work of Burrows et al. (1989) has a related treatment for AVC of rotorbearing systems utilizing a multisensor norm to select the control. Their method also identifies system parameters along with providing AVC. Differences between the present work and theirs include:

- their approach is directly applicable to force type actuators (magnetic bearings) and not to displacement type actuators (piezo-pushers);
- they employ a Euclidean norm, whereas, we have found the "percent change" norm to be more useful since, for instance, the Euclidean norm may not be sensitive to a decrease in vibration at a bearing if the norm is also based on midspan vibration;
- the results in this paper include control of 3 modes whereas the referenced work shows only control of a single mode;
- sampling speed is varied in the current work whereas sensor configuration is varied in the referenced work.

The choice of the type of actuator used in AVC is application dependent. For instance, magnetic bearings have been installed on large diameter turbine generator shafts. These shafts are too large for the DN limitations of rolling element bearings and therefore could not be controlled by piezoelectric actuators which rely on rolling element bearings for force transmission to the rotating shaft. Even in this application though, magnetic bearings still require a catcher (backup) rolling element bearing in case of power failure. Advantages of piezoelectric actuators include:

(*a*) The preload reaction force at the actuator location is

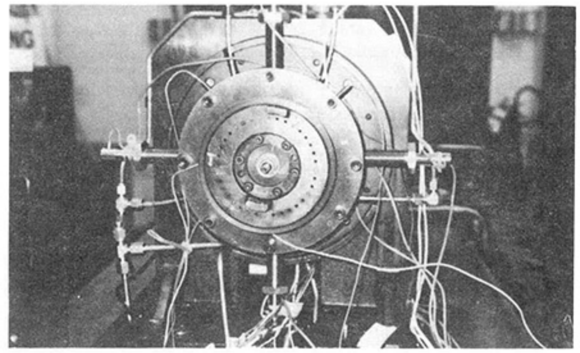

(a) Outboard end view

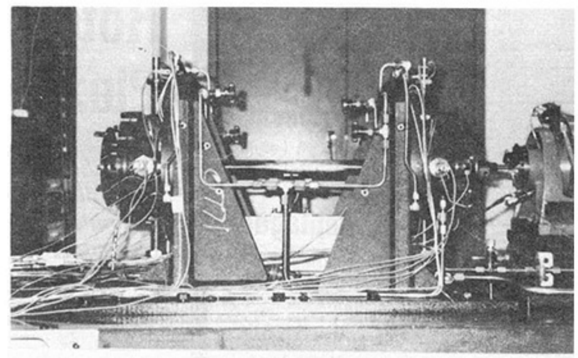

(b) Side view

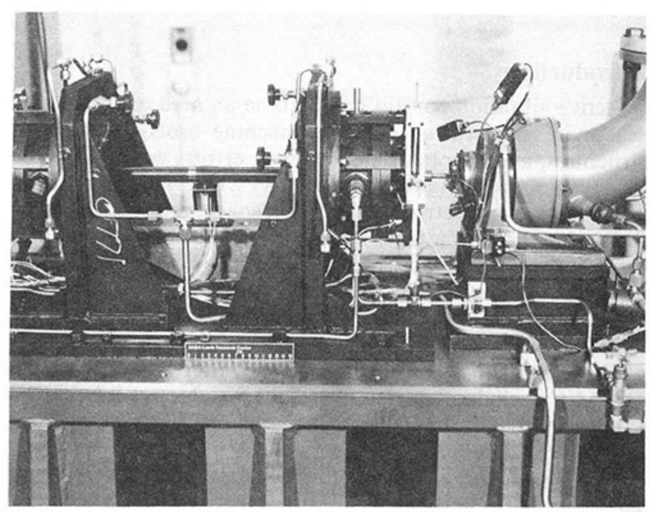

Fig. 1 AVC test rig

Nomenclature

- $\overline{C}/8.0$ = gain of DAC board for derivative feedback
- $\hat{C}$ = zero frequency slope of differentiator frequency response amplitude
- C_{ACT} = equivalent viscous damping coefficient due to derivative feedback
- C_i = capacitance values
- F = Fourier component
- G'_{cp} = gain of variable amplifier in derivative feedback branch
- G'_{KP} = gain of variable amplifier in proportional feedback branch
- $\overline{K}/8.0$ = gain of DAC board for proportional feedback
- K_{ACT} = equivalent direct stiffness coefficient due to proportional feedback
- K_p = stiffness of piezoelectric pusher
- m = mass of bearing housing where actuator is located
- N = number of samples
- R_i = resistance values
- S_A = sensitivity of piezoelectric pusher
- S_D = feedback sensor
- V = vibration norm to be minimized
- V_D = differentiator output voltage
- V_{IN} = input voltage to pusher's amplifier driver
- X = feedback vibration displacement
- α = internal displacement of pusher's idealized model

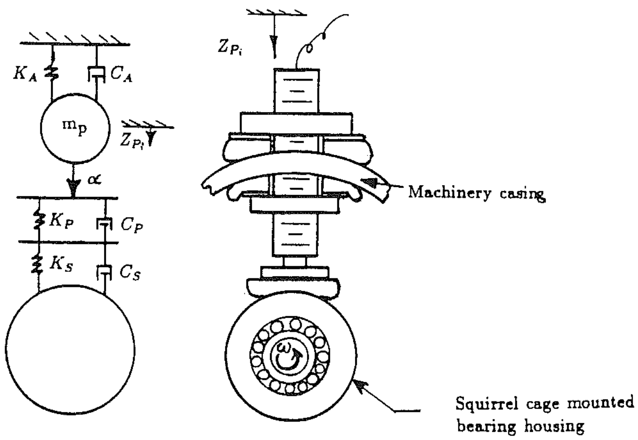

Fig. 2 Ideal representation of a piezoelectric pusher

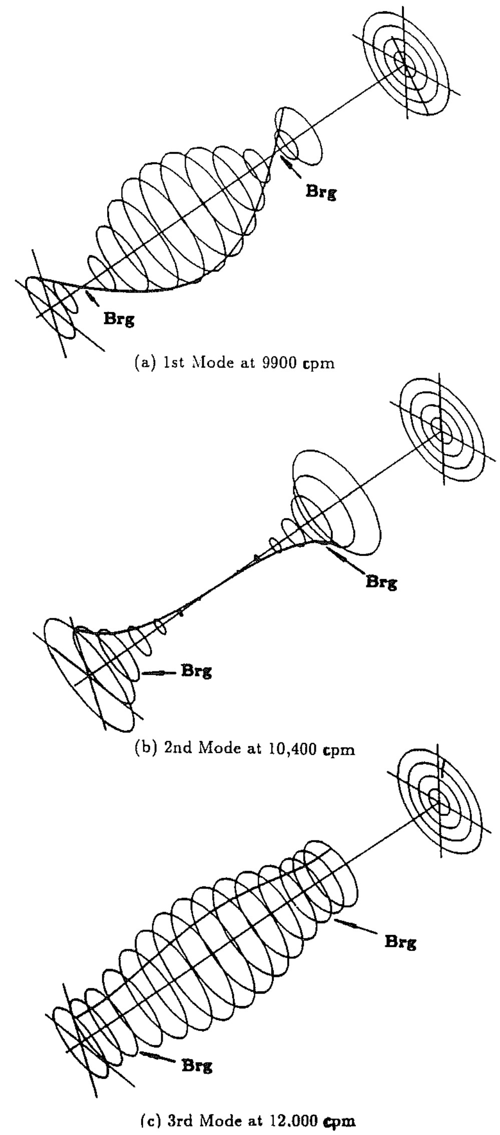

Fig. 3 Simulated modes at 10,000 rpm

counteracted by the passive stiffness of the actuator and the bearing housing support spring and therefore only requires power for vibration control.

(*b*) The shaft will not experience hysteresis related temperature rises due to cyclic stressing of the shaft surface material as it rotates past multiple poles with most magnetic bearings.

(*c*) Piezo actuators do not have the potential for producing shaft current damage or instrumentation electrical interference due to accidental magnetization of rotating or stationary parts.

AVC System

A rotor-bearing system test rig with piezoelectric actuator based AVC has been designed, installed, and tested at NASA Lewis. The test rig consists of an overhung disk at each end of the shaft, two squirrel cage supported bearings, and 4 pusher modules. Each module is defined as a pair of soft-mounted opposing pushers acting on the bearing housing. The rotor is driven by an air turbine and is oil-mist lubricated. The disk and bearing at the turbine end were designated as the inboard disk and inboard bearing, respectively, while the other disk and bearing were referred to as the outboard disk and outboard bearing. Three views of rig are shown in Fig. 1.

The piezoelectric pusher consists of a stack of piezoelectric ceramic discs which are arranged on top of one another and connected in parallel electrically. The stack expands in response to an applied voltage which causes the electric field to point in the direction of polarization for each disc. The extension of the pusher under zero load depends on the number and thickness of the discs and the force for zero extension depends on the cross sectional area of the discs. Figure 2 shows a sketch of a pusher and the corresponding ideal model. The model consists of a prescribed displacement (α) which is proportional to the input voltage and a spring (K_p) representing the stiffness of the stack of piezoelectric discs. The displacement (α) is the "internal" displacement of the pusher which will equal the tip displacement only when the tip is free and the mass of the push rod is neglected. The stiffness, K_A and K_S, and dampings, C_A and C_S, represent the elastomer pad linearized force properties. These pads are employed as mechanical filters to prevent electromechanical system instabilities. The X and Y sets of opposing pushers force the rotating shaft by moving the squirrel cage mounted-rolling element bearing housing as shown in Fig. 2.

Figure 3 shows the first three predicted modes for this system. The first mode has very little amplitude at the bearing locations, while the second mode has a node at midspan and the third mode has sizable amplitude at all locations. These modes were produced with a finite element model of the rotor-bearing system and are in excellent agreement with their measured counterparts.

The rotorbearing system and control system are shown in Fig. 4. The upper diagram illustrates the rotor, actuators, and sensors the lower diagram shows the feedback control system. Signals from the sensors, located at 45 deg angles, are summed to obtain 1.414 times the desired horizontal or vertical displacements. Figure 4 shows the analog controller with a control loop, separated into 2 feedback paths: active damping (ADFT), and active stiffness (ASFT). The former attenuates unbalance response at the resonant frequencies, while the latter is especially useful when the location of the actuators is near the node of a vibration mode. In this case the active stiffness may be used to shift the node and thereby make the active damping more effective. The authors have found this to be an extremely effective approach even when the node is very close to the actuator. Of course, if the actuator is "exactly" on the node it will not be effective in controlling the mode. The effectiveness of sensors and actuators in controlling specific modes may be quantitatively evaluated by considering controllability and observability. Siegwart et al. (1990) defined condition numbers K_o and K_c for this purpose, and then applied them to a milling spindle test case.

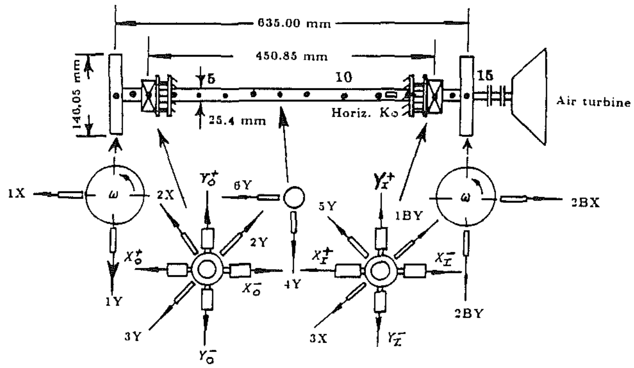

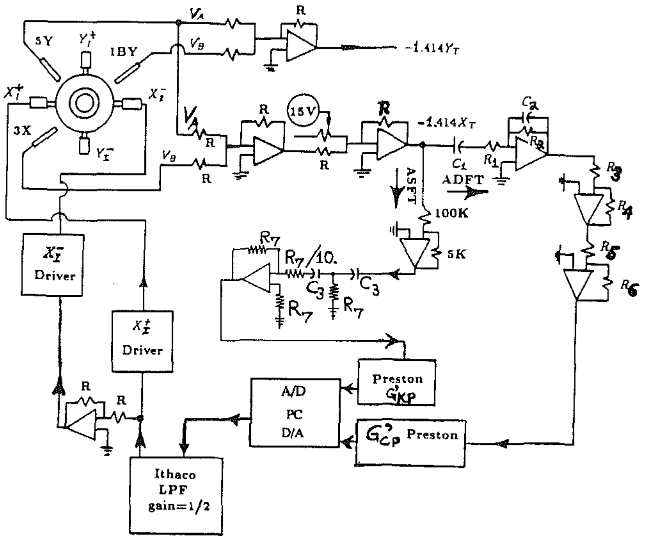

Fig. 4 Control circuit schematic for a pusher module

Four controllers are required for the two directions at each of the two bearing locations. The active damping path (ADFT) consists of a differentiator, two internal amplifiers, and one external (Preston) amplifier of gain G'_{cp}. The active stiffness path (ASFT) consists of an internal amplifier, an inverter, and an external amplifier of gain G'_{KP}. Both paths are routed into the A/D-PC-D/A system which multiplies the ADFT signal by the attenuation factor $\overline{C}/8.0$, multiplies the ASFT signal by the attenuation factor $\overline{K}/8.0$, and then sums the two attenuated signals. The summed signal has its DC bias removed and is then sent into an external 4th order noninverting low pass filter (ITHACO). This filter has a zero-frequency gain of 0.5 and a cutoff frequency that is adjusted to maximize the amount of feedback gain without driving the system unstable. The filter's output signal is sent both to the "+" pusher's driver and in an inverted form to the "−" pusher's driver.

The amount of active damping due to the ADFT feedback can be estimated using the idealized pusher model. For simplicity, the pusher is assumed to be fixed to a rigid casing, reducing Fig. 2 to a 1 dof system. Note that this figure represents only one of the two opposing pushers acting on the bearing housing. The output of the differentiator in Fig. 4 is

$$V_D = -1.414 S_D \hat{C} \omega X \tag{1}$$

where S_D is the probe sensitivity, $\hat{C}\omega$ is the frequency response function of the differentiator over the low frequency range and X is the displacement of the outboard bearing housing in the X direction. Two constant gain amplifiers follow with amplifications R_4/R_3 and R_6/R_5, respectively. The external Preston amplifier provides a gain of G'_{cp} so that its output voltage becomes;

$$V_p = -1.414 G'_{cp} (R_6/R_5)(R_4/R_3) S_D \hat{C} \omega X \tag{2}$$

This signal is attenuated by a factor of $\overline{C}/8.0$ as it passes through the DAC board (A/D-PC-D/A) in Fig. 4. Furthermore the lowpass (ITHACO) filter has a zero frequency attenuation of 0.5 so that the signal entering the pusher driver is

$$V_{IN} = -0.0884 \overline{C} G'_{cp} (R_6/R_5)(R_4/R_3) S_D \hat{C} \omega X \tag{3}$$

The internal displacement (α) of the pusher is approximated by the expression;

$$\alpha = V_{IN}/S_A \tag{4}$$

where S_A is experimentally determined from the equation

$$S_A = V_{IN}/\alpha_F \tag{5}$$

and α_F is the "free-tip" displacement of the pusher due to the input voltage V_{IN}. The internal displacement α of the pusher is thus,

$$\alpha = -0.0884 \overline{C} \, \frac{G'_{cp}(R_6/R_5)(R_4/R_3) S_D \hat{C} \omega X}{S_A} \tag{6}$$

or since $\dot{X} = \omega X$

$$\alpha = -\tilde{G}_c \dot{X} \tag{7}$$

where

$$\tilde{G}_c = 0.0884 \overline{C} \, \frac{G'_{cp}(R_6/R_5)(R_4/R_3) S_D \hat{C}}{S_A} \tag{8}$$

The unknown $\hat{C}$ can be determined by noting that it represents the slope of the magnitude of the frequency response function of the differentiator at $\omega = 0$ (Lin, 1990). The transfer function of a differentiator is

$$TF_{DIFF} = -\frac{R_2 C_1 \lambda}{[R_1 R_2 C_1 C_2 \lambda^2 + (R_1 C_1 + R_2 C_2)\lambda + 1]} \tag{9}$$

Substituting $\lambda = j\omega$, taking the derivative and setting $\omega = 0$, we have

$$\hat{C} = C_1 R_2 \tag{10}$$

Following the active stiffness path in Fig. 4, the output of the Preston amplifier is

$$V_p = -G'_{KP} \times 10.0 \times (5/100) \times 1.414 S_D X \tag{11}$$

where G'_{KP} is the Preston amplifier gain and the factor of 10.0 accounts for the high pass filter gain. This filter is represented in the circuit diagram of Fig. 4 by the op-amp circuit containing R_7 and C_3. This signal is attenuated by a factor of $\overline{K}/8.0$ as it passes through the DAC board (A/D-PC-D/A) in Fig. 4. Furthermore the low pass filter has an attenuation of 0.5 so that the signal entering the pusher driver is

$$V_{IN} = -0.0442 \overline{K} G'_{KP} S_D X \tag{12}$$

Finally the internal displacement of the pusher becomes;

$$\alpha = -0.0442 \overline{K} G'_{KP} \frac{S_D}{S_A} X \tag{13}$$

or

$$\alpha = -\hat{G}_K X \tag{14}$$

where

$$\hat{G}_K = 0.0442 \overline{K} G'_{KP} \frac{S_D}{S_A} \tag{15}$$

The governing differential equation for the bearing housing mass being forced by two opposing pushers is

$$m\ddot{x} = -K_p(x-\alpha) - K_p(x-\alpha) \tag{16}$$

Substitute the feedback law;

$$\alpha = -\hat{G}_c \dot{x} - \hat{G}_K x \tag{17}$$

to obtain

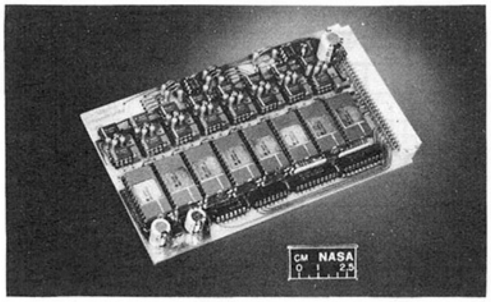

Fig. 5 Hybrid control interface board

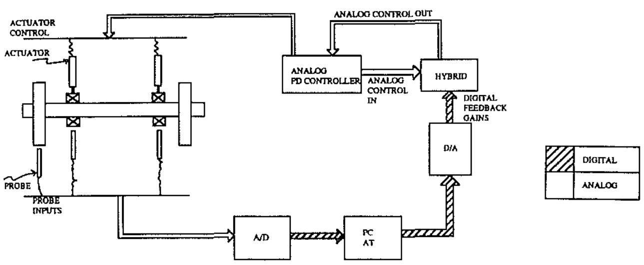

Fig. 6 Schematic of hybrid control hardware configuration

$$m\ddot{x}+C_{ACT}\dot{x}+(2K_p+K_{ACT})x=0 \tag{18}$$

where the active damping is

$$C_{ACT}=2K_p\hat{G}_c \tag{19}$$

and the active stiffness is

$$K_{ACT}=2K_p\hat{G}_K \tag{20}$$

Values for the active stiffness and damping may be approximated from formulae; 8, 15, 19, and 20, for various feedback gains. Identical formulae hold for the Y direction. The interface between the analog controller and the digital computer is the custom-designed hybrid board shown in Fig. 5. The board has 8 analog inputs and provides a summed analog output. Each analog input has a D/A chip so that when a digital value is downloaded to this chip by the computer, it will attenuate the analog input accordingly. The output is thus the sum of individually attenuated inputs. The hybrid board has 8 such chips, forming a DAC array. Attenuation (A) values range between -1 to $+1$. The total attenuation through the DAC board is $A/8.0$.

Two hybrid boards were used in the AVC system: one for the Outboard-X and another for the Outboard-Y controllers. Each board had two inputs for the analog controller stiffness and damping signals. The gains (attenuations) are downloaded to the DAC array from a 12-bit D/A board in the computer.

Six eddy current type-shaft displacement sensors, three in the X-direction (outboard disk, outboard bearing and mid-span), and three in the Y-direction (outboard disk, outboard bearing, and mid-span) are sampled with a 16-bit 250 KHz A/D board. The probes in one direction are sampled simultaneously, followed by the probes in the other direction. All of these six sensor signals are used in evaluating the vibration norm discussed in the next section. The "once per rev" signal triggers a group of 16 samples to be taken from each probe during every shaft revolution. These samples are equally spaced at (360/16) degrees apart. Sampling is paced with a 16-tooth gear wheel mounted at the inboard end of the rotor for the tachometer. Another channel is dedicated to measuring a DC voltage feedback from the turbine speed controller, to monitor the rig speed. Similarly, a dedicated channel exists on the D/A board for controlling turbine speed. Figure 6 shows a schematic of the hardware configuration.

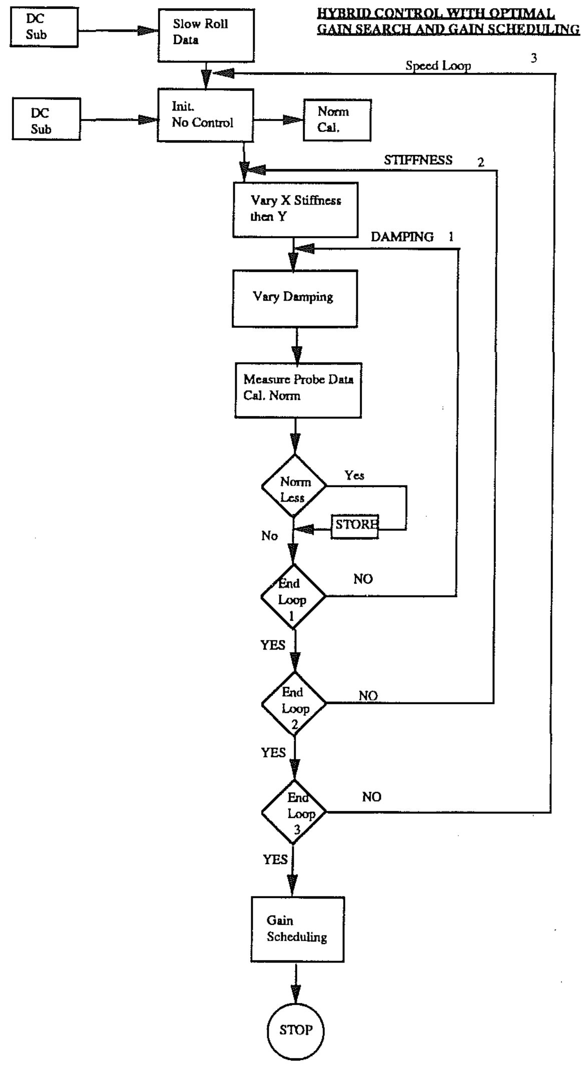

Fig. 7 Flow chart of hybrid optimal control and gain scheduling algorithm

Hybrid Control Algorithm

Figure 7 shows how the control algorithm proceeds in 2 phases: a grid search to identify optimal feedback gains, and then a sequential download of these gains at appropriate speeds during actual operation of the rig.

Optimal feedback gains are selected based on minimizing certain norms of measured vibration. The eddy current shaft displacement signals are corrected for DC bias and slow roll before determining the norms. First it is necessary to eliminate the DC component in the 16 samples taken during each revolution. This is done by evaluating the Fourier term corresponding to the DC (zero) frequency. The discrete Fourier representation of a discrete periodic signal is given by,

$$F(n)=\sum_{K=0}^{N-1} f(k)\,(e^{j2\pi/N})^{-kn} \tag{21}$$

where, $f(k)$ are the discrete-time samples and $F(n)$ are the Fourier components. The DC (constant) component is;

$$F(0)=\frac{1}{N}\sum_{k=0}^{N-1} f(k) \tag{22}$$

The new sequence $\{f(k)-F(0)\}$ will therefore have the DC bias component removed.

Secondly, in order to have a correct measure of the vibration at operating speed, slow-roll data has to be stored and subtracted from each sample. The slow-roll data, being void of dynamic response, is due solely to shaft surface irregularities, material inhomogeneity, and some slight permanent bow of the shaft. The dynamic response due to the bow is neglected as is typically assumed in balancing and other AVC approaches. The computer automatically collects slow-roll samples at low speed, recording their positions relative to the "once per rev" pulse, so that these false vibration samples may be subtracted from samples collected at any other speed. This yields the "corrected" vibration sample:

$$v(k) = v'(k) - d(k) \tag{23}$$

where, $v'(k)$ is the uncorrected vibration sample, and $d(k)$ is the slow-roll sample.

A grid search of discrete stiffness and damping attenuations is conducted to locate the minimum vibration norm. The search proceeds along the range of damping values while keeping the stiffness constant, the latter is then incremented, and the damping is varied again.

A norm is measured at each point in the grid, to provide a measure of the overall vibration of the rotor. The norm utilized here is defined as:

$$V = \sum_i \left[\frac{V_i - V_i^o}{V_i^o} \times 100 \right] \tag{24}$$

$$V_i = \max_K |V_{iK}|, \quad V_i^o = \max_K |V_{iK}^o| \tag{25}$$

where, i is the probe index, K is the time sample index, V_{iK} is the displacement at probe i for sample K (corrected for slow roll and DC bias) in the controlled state, and V_{iK}^o is the displacement at probe i for sample K (corrected for slow roll and DC bias) in the, no-control state. Therefore, the norm V is the sum of the percentage changes in vibration over all six measured probes. The objective is to minimize V, hence if the present V is less than the previous V, the current gains are stored. Once this is repeated over the whole grid the optimal gains will be identified for this operating speed. The turbine is stepped up to the next speed, and the grid search is repeated storing optimal gains at each speed. Once the optimal gains have been identified at each "search" speed, the rig can be run up again and a linear fit applied to the gains between the successive speeds at which the gains were obtained. It is necessary, therefore, that the computer control the rig speed accurately so as not to have a mismatch between search and downloading speeds. A DC voltage from the turbine controller is used as a feedback signal to control speed. Unless mentioned otherwise the scheduling run up rate was set at 25 rpm per second.

Test Results

Many tests were conducted with the system described in the previous sections. The test case results shown here illustrate the typical trends noted in the other runs. Only the outboard pushers (X_0^+, X_0^-, Y_0^+, Y_0^- in Fig. 4) were active for the results described below. The inboard pushers (X_I^+, X_I^-, Y_I^+, Y_I^-) were preloaded against the inboard bearing housing but were not electrically powered. The low pass filters in Fig. 4 had cutoff frequencies of 3,150 and 6,300 hz for the X and Y directions, respectively. In the test results the shaft displacement signals ODX and ODY refer to transducers $1X$ and $1Y$, respectively, in Fig. 4. Similarly $MIDX$ and $MIDY$ refer to transducers $6Y$ and $4Y$, respectively. The vibrations OBX and OBY are formed by summing probes $2X$ and $3Y$, and $2X$ and $2Y$, respectively. Note that probes $2X$, $2Y$, $3X$, $3Y$, $1BY$, and $5Y$ are all oriented 45 deg from either the X or Y axes. The shaft length and diameter are 0.612 meters and 0.0254 meters, respectively. The bearing support (squirrel cage) stiffnesses were both 1.75×10^6 N/M. The disc and bearing weights were 14.0 N and 16.0 N, respectively.

Table 1 Control parameter sets for cases 1-5

Case	$\bar{K}_{init}$	$\Delta\bar{K}$	$\Delta\bar{C}$	$\Delta\bar{N}$ (rpm)	Plot Designation
1	-0.5	0.5	0.5	3000	— — —
2	-0.4	0.5	0.5	1000	———
3	-0.4	0.2	0.2	3000	— - — -
4	-0.4	0.2	0.2	1000*	— - - —
5	-0.4	0.2	0.2	1000**	See Fig. 14

* In addition to these increments case 4 also had searches conducted at 9200, 9400, 9600 and 9800 rpm.

** In addition to these increments case 5 also had searches conducted at 9200, 9400 9600, 9800, 10200, 10400, 10600 and 10800 rpm.

The circuit parameter values in Fig. 4 were;

$R_1 = 1.0$ kΩ
$R_2 = 1.45$ kΩ
$R_3 = 27.0$ kΩ
$R_4 = 2.2$ MΩ
$R_5 = 4.8$ kΩ
$R_6 = 38.7$ kΩ
$C_1 = 9.0$ nF
$C_2 = 0.1$ nF
$S_D = 12{,}000.$v/m
$S_A = 51{,}000.$v/m
$K_p = 4.0 \times 10^6$ N/m (22,800.lb./in)

Substitution of these values into Eqs. (8), (15), (19), and (20) provides the following estimates for the active damping and stiffness for test cases 1–5;

$$\hat{G}_c = 1.78 \times 10^{-4} \bar{C} G'_{cp}(s) \tag{26}$$

$$C_{ACT} = 2K_p \hat{G}_c = 8.12 \bar{C} G'_{cp}(\text{lb.s./in}) = 1{,}422.0 \bar{C} G'_{cp}(\text{N.s./m}) \tag{27}$$

$$\hat{G}_K = 1.04 \times 10^{-2} \bar{K} G'_{KP}(\text{dim}) \tag{28}$$

$$K_{ACT} = 2K_p \hat{G}_K = 474.0 \bar{K} G'_{KP}(\text{lb./in}) = 83{,}200.0 \bar{K} G'_{KP}(\text{N/m}) \tag{29}$$

The external (Preston) amplifier settings were;
X direction

$$G'_{KP} = 500.0 \tag{30}$$

$$G'_{cp} = 2.07 \tag{31}$$

Y direction

$$G'_{KP} = 100.0 \tag{32}$$

$$G'_{cp} = 3.51 \tag{33}$$

The final expressions for the active damping and stiffness become;

$$C_{ACT,X} = 16.81 \bar{C}_x(\text{lb.s./in}) = 2{,}944.0 \bar{C}_x(\text{N.s./m.}) \tag{34}$$

$$K_{ACT,X} = 237{,}000.0 \bar{K}_x(\text{lb./in}) = 4.16 \times 10^7 \bar{K}_x(\text{N./m.}) \tag{35}$$

$$C_{ACT,Y} = 28.5 \bar{C}_Y(\text{lb.s./in}) = 4{,}991.0 \bar{C}_Y(\text{N.s./m.}) \tag{36}$$

$$K_{ACT,Y} = 47{,}400.0 \bar{K}_y(\text{lb./in.}) = 8.32 \times 10^6 \bar{K}_Y(\text{N./m.}) \tag{37}$$

where the values of the stiffness and damping attenuations had the following ranges;

$$0 \le \bar{C}_x \le 1.0, \quad 0 \le \bar{C}_Y \le 1.0 \tag{38}$$

$$0.4 \le \bar{K}_x \le 1.0, \quad -0.4 \le \bar{K}_Y \le 1.0 \tag{39}$$

Table 1 summarizes the search parameter sets for the cases considered in this study. Note that $\bar{K}_{init}$ is the minimum negative stiffness feedback attenuation in the grid. The parameters $\Delta\bar{K}$ and $\Delta\bar{C}$ are step sizes of stiffness and damping attenuations, respectively, while ΔN is the step size of the speed axis which implies the searches were conducted at speeds spaced ΔN apart, beginning at 8,000 rpm and ending at 14,000 rpm. This table also list the plot designation for each case considered in Figs. 8–10.

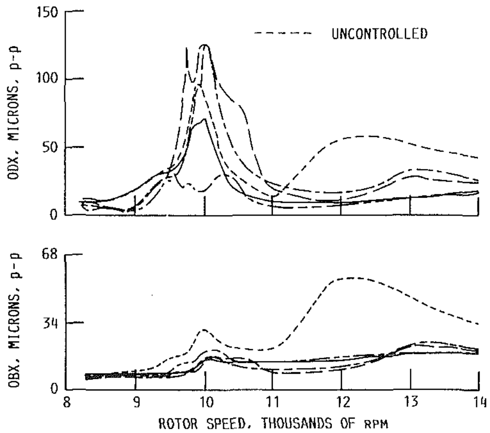

Fig. 8 Synchronous vibration amplitude response for *OBX* and *ODX* probes

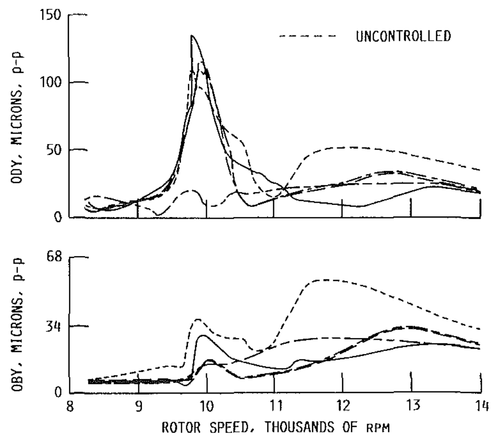

Fig. 9 Synchronous vibration amplitude response for *OBY* and *ODY* probes

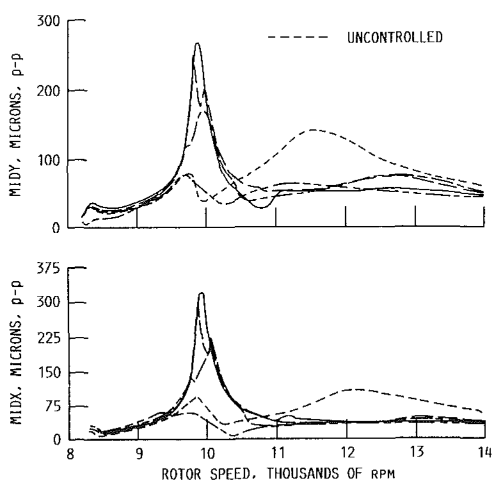

Fig. 10 Synchronous vibration amplitude response for *MIDX* and *MIDY* probes

Figures 8 through 10 show the synchronous responses for different probe locations and different parameter sets. Note that the different cases are distinguished by the line types as defined in Table 1. Cases 1 and 2 have coarse gain grids and Case 1 also has a coarse speed grid. Case 3 has a finer gain grid while maintaining a coarse speed grid. Finally Case 4 has fine gain and speed grids. Cases 1 through 3 show poor control over the first critical. All cases show satisfactory vibration

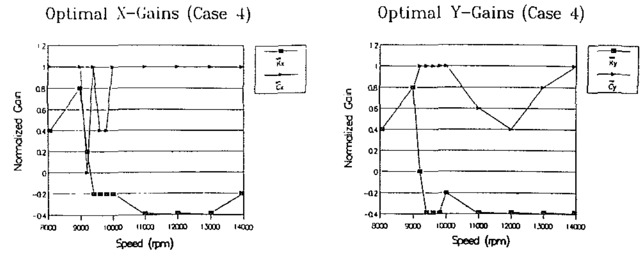

Fig. 11 Optimal *X*- and *Y*-gains vs. speed

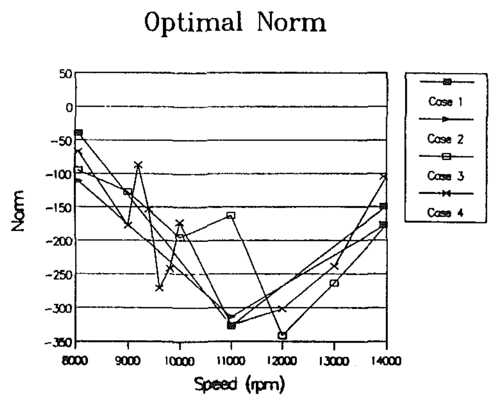

Fig. 12 Optimal norm vs. speed

attenuation over the third critical with cases 2 and 4 being the best. Case 4 shows excellent vibration reduction over the entire speed range. The acceleration rate for the data shown in Figs. 8-10 was 25.rpm/sec.

Figure 11 shows the optimal gains for Case 4 that were downloaded in the *X*- and *Y*-directions of the outboard controllers. These results indicate that near a critical, damping tends to become maximum while the stiffness tends to go negative. Figure 12 shows the optimal norms for Cases 1 to 4, with minimum values occurring near the criticals. Figure 13 shows the norm surfaces, as a function of the $\Delta\overline{K}-\Delta\overline{C}$ grid, are quite different at the two speeds. The difference between the *X* and *Y* surfaces [(*a*) and (*b*) at 9600 rpm or (*c*) and (*d*) at 11,000 rpm] are most likely due to asymmetry in the support or pusher stiffnesses, and in the feedback circuits. The optimum $\overline{C}-\overline{K}$ values are seen to generally occur on the boundary; however, they may also occur in the interior as shown in (*a*).

A fifth case was run in order to investigate the effects of rotor acceleration during the downloading step. The nondimensional stiffness ($\overline{K}$) and damping ($\overline{C}$) increments were 0.2 as in case 4 of Table 1. The "search" speeds for case 5 were identical to those of case 4 with the addition of 10,200, 10,400, 10,600, and 10,800 rpm. The vibration vs. speed plots in Fig. 14 confirm that the feedback gains determined under steady state conditions are still very effective in controlling vibrations at shaft acceleration rates of 25.0, 100.0, and 200.0 rpm/sec.

Conclusions and Recommendations

A key step in any vibration control procedure is to select appropriate feedback gains which minimize some norm of vibration while maintaining a sufficient margin from any instability onset gains. Selection of the feedback gains can be a time consuming process due to the many possible combinations of active stiffnesses, active dampings, and rotor speeds. This paper has presented an automated search procedure to determine optimal feedback gains utilizing A/D, D/A, and digitally controlled attenuation boards. The results showed very significant reductions in vibration levels along the entire test rotor. The optimal feedback gains were shown to be highly dependent on rotor speed which reinforced the need for an effective, automated search procedure. Reducing the rotor speed-search increment in the vicinity of the lightly damped first critical speed was seen to be necessary in suppressing this resonance.

The norm defined in Eq. (24) is a function of the number of probes at which vibration is desired to be reduced. The number of probes is totally arbitrary, other than requiring one sensor being located at each actuator, and is selected by the user. Vibration reduction should only be expected at the probe locations used in the norm definition. Six probes are used in the norm definition and two probes in the feedback circuit for the test described herein.

The grid search method discussed in the paper, although not as elegant as some optimization algorithms, does provide a good estimate of the location of the absolute minimum of the norm. This estimate will, of course, improve as the grid point intervals decrease to zero, providing a more thorough search of the active stiffness-active damping plane. Some of our current research in this area is focused on developing more efficient direct optimization algorithms for constrained minimization of the vibration norm.

Although this paper only presented results for steady state, speed dependent control the authors' previous work (Palazzolo et al., 1991) clearly demonstrates its effectiveness for time transient control. The time transient tests employed the same feedback gains as utilized in the steady state response tests. It

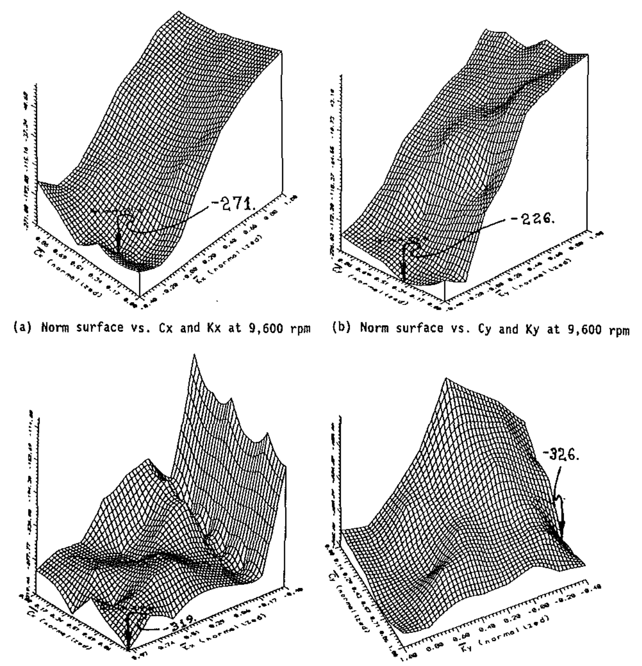

(a) Norm surface vs. Cx and Kx at 9,600 rpm (b) Norm surface vs. Cy and Ky at 9,600 rpm

(c) Norm surfaces vs. $\bar{C}x$ and $\bar{K}x$ at 11,000 rpm (d) Norm surface vs. $\bar{C}y$ and $\bar{K}y$ at 11,000 rpm

Fig. 13 Optimal norm surfaces for the x and y planes at 9,600 and 11,000 rpm

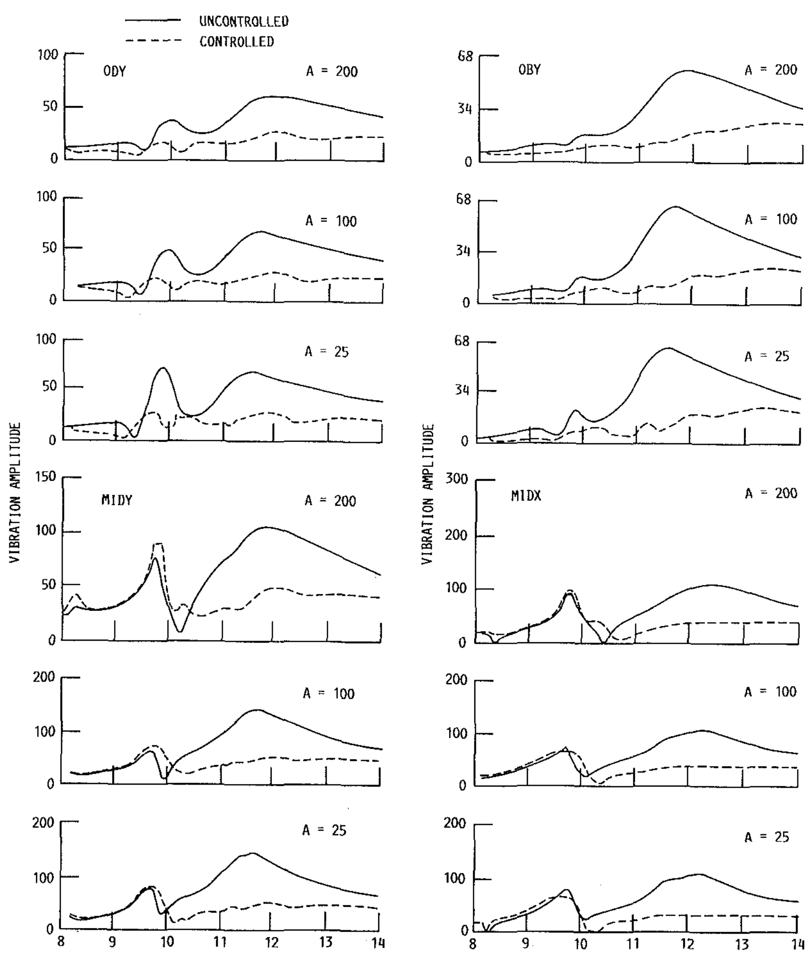

Fig. 14 Synchronous vibration amplitude in (microns, p-p) at various probes and acceleration rates A (rpm/sec), for gain scheduling case 5

should not be concluded that steady state gains will be effective for all transient cases; however, this was the result for the sudden imbalance tests conducted by the authors at NASA. The piezoelectric actuator based AVC system discussed here for the laboratory rotor has now been successfully applied to the transmission shaft line of a gas turbine engine test stand at NASA Lewis. Results from those tests will be forthcoming in a future publication. The test stand application required a more powerful pusher with force and stiffness ratings of 3000.N and 33×10^6 N/M, respectively. The ratings of the pushers described in the present paper were 400.N (Force) and $4. \times 10^6$ N/M (Stiffness). Increased force and stiffness in the pusher require larger pusher diameters and more powerful amplifiers. Although this paper only presents results for a hybrid controller wherein the P and D gains of the analog feedback are set digitally we have implemented the same feedback entirely with digital components. The DSP based digital system is more flexible in implementing various control algorithms; however, a tradeoff occurs because of the additional phase lag that results from the finite sampling time. The results from the digital control system studies will be presented in a forthcoming publication.

Other AVC algorithms have been developed for application to magnetically suspended rotors. Notable among these are the H^∞ control presented in Fujita (1990) and Herzog (1990), and the feedforward control in Ming Chen (1991). The former method holds out the promise of control over a wide frequency range insuring robustness of the controller even for transient disturbances. A drawback of this approach is the iterative solution procedure required to obtain the desired controller. The latter approach cleverly balances the rotor via the influence coefficient method utilizing the magnetic bearing as an actuator, thereby avoiding the addition or removal of weights to the rotor. This approach appears to be very effective if the predicted correction forces fall within the force range of the actuators. The most attractive feature of feedforward control is the avoidance of stability problems which accompany feedback control. However, the feedforward control will be ineffective in suppressing vibrations of a mode with nodes "near" the actuators, as those with field balancing experience will quickly realize. Feedback control can relocate these nodes to make the actuator more effective in suppressing the mode. Furthermore, feedback control will suppress not only synchronous vibration but also nonsynchronous vibration. The authors do not envision any special difficulty in applying H^∞ or feedforward control to actively controlled rotor bearing system, with piezoelectric actuators.

The authors have applied piezo-pusher AVC to a laboratory test rotor and to an engine test stand and have found it to be very effective in both cases. We feel that this technology is generally applicable within the constraints of allowable actuator envelopes and electrical power requirements, constraints which are also imposed on magnetic bearings.

Acknowledgments

The authors gratefully acknowledge the funding for this research provided by NASA Lewis, the Texas A&M Turbomachinery Research Consortium, and the U.S. Army. Sincere appreciation is also extended to the following people for their technical assistance: John Ropchock, Dr. Gerald Brown, and Tom Lokatos of NASA, and Lifang Fu and Doug Roever of Texas A&M. Special appreciation is extended to Professor Heinz Ulbricht (Technische Universität München), Mr. Steve Posta (NASA-retired) and Charles Finaly (Sverdrup) for development of the DAC array boards and instructions on their use, and to Dr. Reng Rong Lin (AC Compressors) whose previous research remains an invaluable reference. Finally the authors thank Ms. Wendy Harding for her excellent preparation of this manuscript.

References

1 Burrows, C. R., Sahinkaya, M. N., and Clements, S., 1989, "Active Vibration Control of Flexible Rotors: An Experimental and Theoretical Study," *Royal Society of London Proc.*, Series A, pp. 123–146.

2 Crawley, E. F., and de Luis, J., 1983, "Experimental Verification of Piezoelectric Actuators for Use in Precision Space Structures," AIAA Paper 83-0878.

3 Crawley, E. F., and de Luis, J., 1985, "Use of Piezoceramics as Distributed Actuators in Large Space Structures," *Proceedings of the 26th Structures, Structural Dynamics, and Materials Conference*, Part 2, AIAA-ASME-ASCE, Orlando, Florida, April, pp. 126–133.

4 Feng, G., and Xin, N., 1986, "Automatic Control of the Vibration of the Flexible Rotor with Microcomputer," Int. Conf. on Rotordynamics, IFTOMM and JSME, Tokyo, Sept., pp. 14–17.

5 Fujita, M., Matsumura, F., and Shimizu, M., 1990, "H^∞ Robust Control Design for a Magnetic Suspension System," 2nd Inter. Symposium on Magnetic Bearings, Tokyo, Japan, July 12–14, pp. 349–356.

6 Gondholekar, V., and Holmes, R., 1984, "Design of Electromagnetic Bearing for Vibration Control of Flexible Transmission Shaft," Rotordynamic Instability Problem in High Performance Turbomachinery, Texas A&M Univ., May.

7 Heinzmann, J. D., Flack, R., and Lewis, D., 1980, "The Implementation of Automatic Vibration Control in High Speed Rotating Test Facility," Univ. of Virginia Report UVA/464761/MAE80/160.

8 Herzog, R., and Bleuler, H., 1990, "Stiff AMB Control Using an H^∞ Approach," 2nd Int. Symposium on Magnetic Bearings, Tokyo, Japan, July 12–14, pp. 343–348.

9 Humphris, R., et al., 1986, "Effect of Control Algorithms on Magnetic Journal Bearing Properties," ASME *Journal of Engineering for Gas Turbines and Power*, Oct., Vol. 108, pp. 624–632.

10 Lin, Reng R., 1990, "Active Vibration Control of Rotorbearing Systems Utilizing Piezoelectric Pushers," Texas A&M University Dissertation, Mechanical Engineering Department, August.

11 Lin, R. R., Palazzolo, A. B., Kascak, A. F., and Montague, G. T., 1991, "Electromechanical Simulation and Testing of Actively Controlled Rotordynamic Systems with Piezoelectric Actuators," ASME Gas Turbine Conference, Orlando, FL., accepted for ASME Journal publication.

12 Matsubara, T., Yamamoto, H., and Mizumoto, H., 1989, "Chatter Suppression by Using Piezoelectric Active Dampers," Rotatory Machinery Dynamics, DE-Vol. 18-1, 12th Biennial Conference on Mechanical Vibration and Noise, Montreal, Quebec, Canada, September, pp. 79–83.

13 Ming Chen, H., 1991, "Virtual Balancing of Rotors Supported by Magnetic Bearings," 13th Biennial ASME Vibration Conference, DE-Vol. 35, pp. 65–68.

14 Nikolajsen, J., Holmes, R., and Gondholekar, V., 1979, "Investigation of an Electromagnetic Damper for Vibration Control of a Transmission Shaft," *Proc. Inst. Mech. Engr.*, Vol. 193, pp. 331–336.

15 Palazzolo, A. B., Lin, R. R., Kascak, A. F., Montague, J., and Alexander, R. M., 1991, "Test and Theory for Piezoelectric Actuator—Active Vibration Control of Rotating Machinery," ASME JOURNAL OF VIBRATION AND ACOUSTICS, April, Vol. 113, pp. 167–175, ASME Conf., Montreal, Canada, September, 1989.

16 Palazzolo, A. B., Lin, R. R., Kascak, A. F., Montague, J., and Alexander, R. M., 1989, "Piezoelectric Pushers for Active Vibration Control of Rotating Machinery," ASME JOURNAL OF VIBRATION, ACOUSTICS, STRESS, AND RELIABILITY IN DESIGN, Vol. 111, July, pp. 298–305.

17 Salm, J., and Schweitzer, G., 1984, "Modelling and Control of a Flexible Rotor with Magnetic Bearings," IMechE., Third Int. Conf. Vibrations in Rotating Machinery, York, Paper No. C277/84, pp. 553–561.

18 Siegwart, R., Larsonneur, R., and Traxler, A., 1990, "Design and Performance of a High Speed Milling Spindle in Digitally Controlled Active Magnetic Bearings," Second International Symposium on Magnetic Bearings, July 12–14, Tokyo, Japan, pp. 197–204.

19 Stjernstrom, S. C., 1987, "Active Vibration Control Using Piezoceramic Transducers," Texas A&M University Thesis, Mechanical Engineering Department, December.

20 Tzou, H. S., 1987, "Active Vibration Control of Flexible Structures Via Converse Piezoelectricity," Presented at the 20th Midwestern Mechanics Conference, 8/31–9/2, 1987, Developments in Mechanics, pp. 1201–1206, Vol. 14-c.

21 Ulbrich, H., and Althous, J., 1989, "Actuator Design for Rotor Control," DE-Vol. 18-2, 12th Biennial Conference on Mechanical Vibration and Noise, Montreal, Canada, pp. 17–22.

22 Weise, D., 1985, "Active Magnetic Bearings Provide Closed Loop Servo Control for Enhanced Dynamic Response," *Proc. 27th IEEE Machine Tool Conf.*, October.